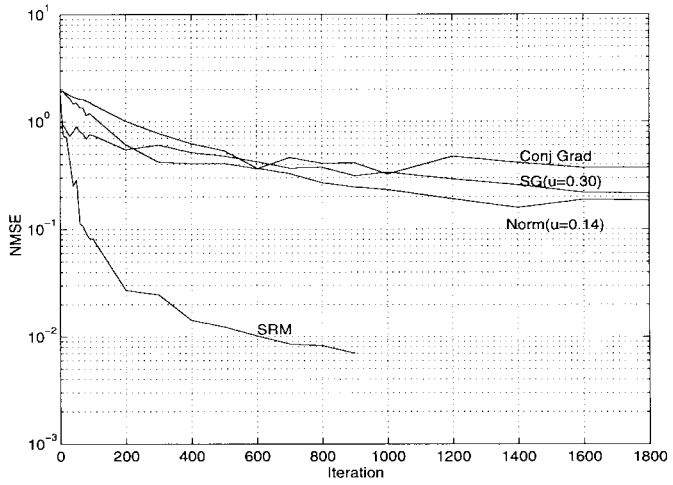

Fig. 5. Comparison of the SRM-based algorithms for the "Bad" channel, SNR $= 10$ dB. SG: Standard stochastic gradient algorithm. Norm: Normalized stochastic gradient algorithm. SRM: Off-line SRM algorithm of [3], where S_k is obtained at time k by averaging all of the data through time k to estimate ensemble averages. Conj Grad: Conjugate gradient algorithm. The results are averaged over 200 sample trials.

where λ_i is the eigenvalue corresponding to the ith eigenvector of S_Z. If the initial guess is chosen on the unit circle (i.e., $\|\hat{\boldsymbol{h}}_0\| = 1$), the fact that the magnitude of $\hat{\boldsymbol{h}}_k$ is nondecreasing and (5) can be used to show [10] that convergence occurs in all of the modes if $\mu < (2/\lambda_{\max})$, where $\lambda_{\max}$ is the largest eigenvalue of S_Z. Since $\lambda_{\max}$ is difficult to obtain, the conservative rule $\mu \leq (2/\mathrm{tr}(S_Z))$ is used instead, where $\mathrm{tr}(S_Z) = L(N-1)\ \Sigma_{i=0}^{N-1}\ E|y_i(k)|^2 - LN(N-1)\sigma^2$, which can be readily estimated if the signal-to-noise ratio is known.

Equation (5) suggests defining a normalized algorithm to eliminate the $\|\hat{\boldsymbol{h}}_{k-1}\|^2$ dependence in the convergence condition. The normalized algorithm is obtained by using a variable gain factor $\mu\|\hat{\boldsymbol{h}}_{k-1}\|^2$ at the kth step. Employing this variable gain factor yields

$$\hat{\boldsymbol{h}}_k = \hat{\boldsymbol{h}}_{k-1} - \mu \frac{(\|\hat{\boldsymbol{h}}_{k-1}\|^2 S_k^* \hat{\boldsymbol{h}}_{k-1} - (\hat{\boldsymbol{h}}_{k-1}^T S_k \hat{\boldsymbol{h}}_{k-1}^*)\hat{\boldsymbol{h}}_{k-1})}{\|\hat{\boldsymbol{h}}_{k-1}\|^2} \quad (6)$$

which is (3) of the main text. The convergence analysis of this normalized stochastic gradient update follows similarly and implies convergence if $\mu < (2/\lambda_{\max})$.

References

[1] H. Liu, G. Xu, and L. Tong, "A deterministic approach to blind equalization," in *Conf. Rec. Twenty-Seventh Asilomar Conf. Signals, Syst., Comput.*, 1993, pp. 751–755.

[2] L. Baccalá and S. Roy, "Time-domain blind channel identification algorithms," in *Proc. 1994 Conf. Inform. Sci. Syst.*, vol. 2, pp. 863–867.

[3] S. Schell and D. Smith, "Improved performance of blind equalization using prior knowledge of transmitter filter," in *Conf. Rec. 1994 IEEE Mil. Commun. Conf.*, vol. 1, pp. 128–132.

[4] L. Tong, G. Xu, and T. Kailath, "Blind identification and equalization based on second-order statistics: A time domain approach," *IEEE Trans. Inform. Theory*, vol. 40, pp. 340–349, Mar. 1994.

[5] E. Moulines, P. Duhamel, J. Cardoso, and S. Mayrargue, "Subspace methods for the blind identification of multichannel FIR filters," *IEEE Trans. Signal Processing*, vol. 43, pp. 516–525, Feb. 1995.

[6] L. Baccalá and S. Roy, "A new blind time-domain channel identification method based on cyclostationarity," *IEEE Signal Processing Lett.*, vol. 1, pp. 89–91, June 1994.

[7] H. Zeng and L. Tong, "Blind channel estimation using the second-order statistics: Algorithms," *IEEE Trans. Signal Processing*, vol. 45, pp. 1919–1930, Aug. 1997.

[8] M. Tsatsanis and G. Giannakis, "Multirate filter banks for code-division multiple access systems," *Proc. 1995 Int. Conf. Acoust., Speech, Signal Process.*, vol. 2, pp. 1484–1487.

[9] ——, "Optimal decorrelating receivers for DS-CDMA systems: A signal processing framework," *IEEE Trans. Signal Processing*, vol. 44, pp. 3044–3055, Dec. 1996.

[10] D. Goeckel, A. Hero, III, and W. Stark, "Blind channel identification for direct-sequence spread-spectrum systems," in *Conf. Rec. 1995 IEEE Mil. Commun. Conf.*, pp. 368–372.

[11] M. Stojanovic, "Recent advances in high-speed underwater acoustic communications," *IEEE J. Oceanic Eng.*, vol. 21, pp. 125–136, Apr. 1996.

[12] P. Thompson, "An adaptive spectral analysis technique for unbiased frequency estimation in the presence of white noise," in *Conf. Rec. Thirteenth Asilomar Conf. Circuits, Syst., Comput.*, 1979, pp. 529–533.

[13] M. Larimore and R. Calvert, "Convergence studies of Thompson's unbiased adaptive spectral estimator," in *Conf. Rec. Fourteenth Asilomar Conf. Circuits, Syst., Comput.*, 1980, pp. 258–262.

[14] H. Chen, T. Sarkar, S. Dianat, and J. Brulé, "Adaptive spectral estimation by the conjugate gradient method," *IEEE Trans. Acoust., Speech, Signal Processing*, vol. ASSP-34, pp. 272–284, Apr. 1986.

[15] G. Mathew, S. Dasgupta, and V. Reddy, "Improved Newton-type algorithm for adaptive implementation of Pisarenko's harmonic retrieval method and its convergence analysis," *IEEE Trans. Signal Processing*, vol. 42, pp. 434–437, Feb. 1994.

[16] X. Yang, T. Sarkar, and E. Arvas, "A survey of conjugate gradient algorithms for solution of extreme eigen-problems of a symmetric matrix," *IEEE Trans. Acoust., Speech, Signal Processing*, vol. 37, pp. 1550–1555, Oct. 1989.

Cascaded Power Symmetric IIR Filter Banks and Continuity Constrained Adaptive Algorithms for Acoustic Echo Cancellation in Subbands

Oğuz Tanrıkulu and Anthony G. Constantinides

***Abstract*— The problem of aliasing in subband acoustic echo cancellation (AEC) is addressed. Filter banks with implicit notch filtering are derived from cascaded power symmetric–infinite impulse response (CPS-IIR) filters. It is shown that adaptive filters used with these filter banks must be coupled via continuity constraints to reduce the aliasing in the residual echo. A continuity constrained NLMS algorithm is therefore proposed and evaluated.**

***Index Terms*—Adaptive filters, echo suppression, IIR digital filters.**

I. Introduction

Teleconferencing systems and hands-free mobile terminals use acoustic echo cancellation (AEC) for high-quality full-duplex speech communication [1]. AEC in subbands is an effective way of reducing the computational complexity [2], [3]. However, the performance is

Manuscript received January 27, 1997; revised January 27, 1998. This work was supported in part by the U.K., EPSRC Research Project GR/K48617 "Multi-rate Echo Cancellation." The associate editor coordinating the review of this paper and approving it for publication was Prof. P. P. Vaidyanathan.

O. Tanrıkulu is with DSP Software Engineering, Inc., Bedford, MA 01730 USA.

A. G. Constantinides is with the Signal Processing and Digital Section, Department of Electrical and Electronic Engineering, Imperial College of Science, Technology, and Medicine, London, U.K.

Publisher Item Identifier S 1053-587X(98)05232-5.

TABLE I
ALLPASS COEFFICIENTS OF $H_0(z)$ AND $\breve{H}_0(z)$

All-pass coef.	$\alpha_{0,0}$	$\alpha_{0,1}$	$\alpha_{0,2}$	$\alpha_{1,0}$	$\alpha_{1,1}$	$\alpha_{1,2}$
$H_0(z)$	0.778242	0.118008	-	0.408292	-	-
$\breve{H}_0(z)$	0.666472	0.293250	0.037332	0.879585	0.472206	0.141475

limited due to the aliasing in the neighboring subbands. When highly selective PS-IIR filters are used, aliasing appears as perceptually disturbing narrowband components in the residual echo [4]. The phase distortion on the reconstructed near-end speech is also significant around subband edges. Therefore, notch filters were used in [4] to deal with both problems.

The filter banks proposed in this correspondence perform notch filtering implicitly by reducing the computational complexity and delay in the analysis and synthesis banks. It is shown that the adaptive filters operating in neighboring subbands must be coupled via continuity constraints in order to ensure the existence of implicit notches in the residual echo. The widely used NLMS algorithm is, therefore, reformulated, and the resulting AEC system is evaluated with synthetic and real signals.

II. POWER SYMMETRIC IIR FILTER BANKS

A PS-IIR filter has the transfer function

$$H_0(z) = \frac{A_0(z^2) + z^{-1}A_1(z^2)}{2}$$
$$A_m(z^2) = \prod_{n=0}^{P_m-1} \frac{\alpha_{m,n} + z^{-2}}{1 + \alpha_{m,n}z^{-2}}, \qquad m = 0, 1 \tag{1}$$

where $A_m(z^2)$ are cascaded second-order allpass stages, and $\alpha_{m,n}$ are real coefficients. Methods for designing highly selective lowpass PS-IIR filters can be found in [4]–[6]. PS-IIR filters satisfy the *power symmetric property*,[1], $H_0(z)H_0^*(z^{-1}) + H_0(-z)H_0^*(-z^{-1}) = 1$, and the *numerator symmetric property* as described in [5]. Once a prototype lowpass filter is available, the corresponding mirror image highpass filter is given by $H_1(z) = H_0(-z)$. Let $z = e^{j\theta}$; then, $|H_0(\pi/2)| = |H_1(\pi/2)| = 1/\sqrt{2}$ independent of $\alpha_{i,j}$, and therefore, a binary-tree subband decomposition is necessary. The multirate analysis bank (MAB) and the multirate synthesis bank (MSB) can be efficiently implemented in polyphase form [4], [5].

When the synthesis bank filters are defined as $G_0(z) = 2H_0(z)$, and $G_1(z) = -2H_1(z)$ for aliasing cancellation, the input–output transfer function of the cascaded MAB and MSB is given by $T(z) = z^{-1}A_0(z^2)A_1(z^2)$ [5]. There is no amplitude distortion since $T(z)$ is allpass. There is, however, phase distortion, and it is most significant around $\theta = (\pi/2)$ [4]. In [4], distributed notch filters (DNF's) are inserted at the input of each binary MAB so that the spectral components around the subband edges are attenuated over a narrow bandwidth. The basic DNF is designed from a PS-IIR filter [4], and it has the transfer function $N(z) = (1/2)[(\gamma_2 + \gamma_1 z^{-1} + z^{-2}/1 + \gamma_1 z^{-1} + \gamma_2 z^{-2})\ (\gamma_2 - \gamma_1 z^{-1} + z^{-2}/1 - \gamma_1 z^{-1} + \gamma_2 z^{-2}) + (\zeta + z^{-2}/1 + \zeta z^{-2})]$. The parameters of a typical DNF are $\zeta = 0.854\,081, \gamma_1 = 0.127\,101, \gamma_2 = 0.919\,032$. Note that highly selective PS-IIR filters can be difficult to design for large (P_0, P_1). An alternative design based on cascaded PS-IIR filters is described in the next section.

[1]The power symmetric property and the paraunitary property are equivalent for two-channel causal FIR QMF filter banks. See ([5, Sec. 14.9]) for an extended discussion on the paraunitary property for m-channel $(m > 2)$ IIR filter banks.

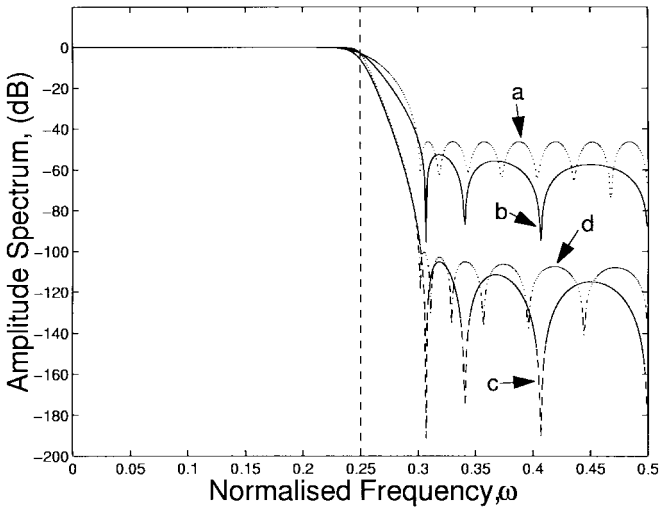

Fig. 1. Amplitude spectra of various prototype filters. (a) PR-FIR (32-taps). (b) PS-IIR; $H_0(z)$. (c) CPS-IIR; $H_0^2(z)$. (d) PS-IIR; $\breve{H}_0(z), \omega = (\theta/2\pi)$.

III. CASCADED PS-IIR (CPS-IIR) FILTER BANKS

Let $H_0(z)$ be a lowpass, PS-IIR filter. Then, the p-fold CPS-IIR transfer function

$$H_0^p(z) = \frac{[A_0(z^2) + z^{-1}A_1(z^2)]^p}{2^p}, \qquad p = 2, 3, 4, \cdots \tag{2}$$

is also lowpass. The passband sensitivity of $H_0(z)$ is very low [7], [8], and therefore, $H_0^p(z)$ has an acceptable passband ripple for small p. Moreover, the stopband attenuation is p times higher, as shown in Fig. 1, where $(P_0, P_1) = (2, 1)$, and the stopband frequency is $\theta_s = 1.885$ rad for $H_0(z)$ and $p = 2$. A PS-IIR filter $\breve{H}_0(z)$ with an amplitude spectrum similar to that of $H_0^2(z)$ is designed with $(P_0, P_1) = (3, 3)$ and $\theta_s = 1.885$ rad. The allpass coefficients of $H_0(z)$ and $\breve{H}_0(z)$ are tabulated in Table I. A 32-tap *perfect reconstruction* (PR) FIR filter is also designed [5], whose amplitude spectrum is also in Fig. 1.

After expanding (2), we have

$$H_0^p(z) = \frac{1}{2^p} \sum_{i=0}^{p} \binom{p}{p-i} A_0^{p-i} A_1^i z^{-i} \tag{3}$$

where we denote $A_0(z^2)$ by A_0 and $A_1(z^2)$ by A_1 for convenience, and $\binom{m}{n} \stackrel{\text{def}}{=} (m!/n!(m-n)!)$.

Remark 1 (Polyphase Structure): Assume that p is even; then, from (3), $H_0^p(z) = (\tilde{A}_0(z^2) + z^{-1}\tilde{A}_1(z^2)/2$, where

$$\tilde{A}_0(z^2) = \frac{1}{2^{p-1}} \sum_{i=0}^{p/2} \binom{p}{p-2i} A_0^{p-2i} A_1^{2i} z^{-2i} \tag{4}$$

$$\tilde{A}_1(z^2) = \frac{1}{2^{p-1}} \sum_{i=0}^{p/2-1} \binom{p}{p-2i-1} A_0^{p-2i-1} A_1^{2i+1} z^{-2i}. \tag{5}$$

The corresponding mirror image highpass filter is therefore given by $H_1^p(z) = (\tilde{A}_0(z^2) - z^{-1}\tilde{A}_1(z^2)/2)$, and the resulting filter bank can be implemented in polyphase form, which is shown in Fig. 2 for $p = 2$.

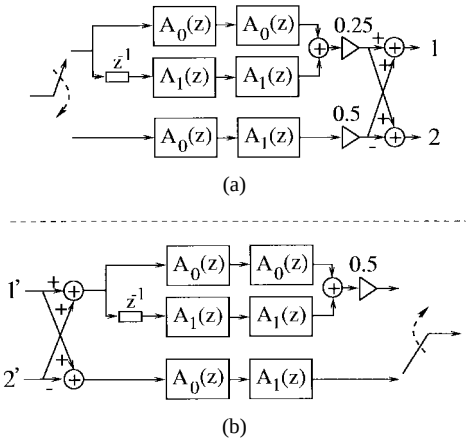

Fig. 2. Polyphase implementation of the multirate CPS-IIR filter bank $(p = 2)$. (a) Analysis bank. (b) Synthesis bank.

Theorem 1: Consider (2), and let p be even with the analysis bank filters defined as $H_0^p(z)$ and $H_1^p(z)$. Let the synthesis bank filters be $G_0(z) \stackrel{\text{def}}{=} 2H_0^p(z)$, and $G_1(z) \stackrel{\text{def}}{=} -2H_1^p(z)$. Then, i) the transfer function of the cascaded MAB and MSB is given by

$$\tilde{T}(z) = z^{-1}\tilde{A}_0(z^2)\tilde{A}_1(z^2) \tag{6}$$

and ii) we have $((p/2)$: odd $\Rightarrow \tilde{A}_0(z^2)\lfloor_{z=e^{j(\pi/2)}} = 0)$, and $((p/2)$: even $\Rightarrow \tilde{A}_1(z^2)\lfloor_{z=e^{j(\pi/2)}} = 0)$. Hence, $\tilde{T}((\pi/2)) = 0$ for all even p, indicating that there is a notch at the output of the cascaded MAB and MSB at $\theta = (\pi/2)$.

The proof of i) is by analogy with $T(z) = z^{-1}A_0(z^2)A_1(z^2)$ for the PS-IIR filters. The proof of ii) follows after evaluating (4) and (5) at $\theta = (\pi/2)$. Note that when p is odd, the CPS-IIR filter bank can be expressed in polyphase form. However, it can be verified that there is no notch at $\theta = (\pi/2)$.

The bandwidth of the implicit notch in relation to the allpass coefficients of the prototype lowpass PS-IIR filter $H_0(z)$ is an important design parameter. An approximate expression for this parameter is obtained below for $p = 2$. From (4)–(6), we have $|\tilde{T}(\theta)| = \frac{1}{2}\,|A_0^2(\theta) + e^{-j2\theta}A_1^2(\theta)|$. Furthermore, using the allpass property $A_0(\theta) = e^{j\phi_0(\theta)}$, $A_1(\theta) = e^{j\phi_1(\theta)}$, we get $|\tilde{T}(\epsilon+(\pi/2))| = |\cos(\epsilon+(\pi/2)+\phi_0(\epsilon+(\pi/2))-\phi_1(\epsilon+(\pi/2)))|$. At the 3-dB point, $|\tilde{T}(\epsilon+(\pi/2))| = 1/\sqrt{2}$, or equivalently, $f(\epsilon) \stackrel{\text{def}}{=} \epsilon+(\pi/4)+\phi_0(\epsilon+(\pi/2)) - \phi_1(\epsilon+(\pi/2)) = 0$. The phase responses $\phi_m(\theta), m = 0, 1$ are given by [4] $\phi_m(\theta) = -2\,\Sigma_{n=0}^{P_m-1}\,\arctan\,((1-\alpha_{m,n}/1+\alpha_{m,n})\tan(\theta))$ from which it can be shown that

$$\left.\frac{\partial\phi_m\left(\epsilon+\frac{\pi}{2}\right)}{\partial\epsilon}\right|_{\epsilon=0} = -2\sum_{n=0}^{P_m-1}\frac{1+\alpha_{m,n}}{1-\alpha_{m,n}}, \left.\frac{\partial^2\phi_m\left(\epsilon+\frac{\pi}{2}\right)}{\partial\epsilon^2}\right|_{\epsilon=0} = 0\,. \tag{7}$$

Furthermore, we also have $f(0) = (\pi/4)$. Therefore, from the truncated Taylor series of $f(\epsilon)$ around $\epsilon = 0$, the bandwidth corresponding to the 3-dB points of the notch is approximately obtained as

$$BW \stackrel{\text{def}}{=} 2\,|\epsilon| \approx \frac{\frac{\pi}{2}}{\left|1 - 2\sum_{n=0}^{P_0-1}\frac{1+\alpha_{0,n}}{1-\alpha_{0,n}} + 2\sum_{n=0}^{P_1-1}\frac{1+\alpha_{1,n}}{1-\alpha_{1,n}}\right|}. \tag{8}$$

For instance, the BW corresponding to the CPS-IIR filter $H_0^2(z)$ in Fig. 1 is 0.157 rad. From (8), we have $BW \approx 0.122$ rad. The approximation error occurs over 1.11% of the entire bandwidth; $\theta \in [0, \pi]$.

IV. Generic Two-Band AEC Unit

In this section, we obtain the conditions such that the aliasing at the output a generic two-band AEC unit [4] is attenuated by an implicit notch filtering operation. Let us make the following definitions in the Z domain: $X(z)$ is the loudspeaker signal. $S(z)$ is the acoustic echo path that we take as linear and time-invariant [3]. Then, $D(z) = S(z)X(z) + Q(z)$ is the signal captured by the microphone, where $S(z)X(z)$ is the acoustic echo, and $Q(z)$ is the near-end signal. $E(z)$ is the fullband residual echo signal, and $\boldsymbol{C}(z)$ is a 2×2 predictor matrix whose off-diagonal terms are taken as zero since cross-channel identification is not performed [3], [4]. Define the vectors $\boldsymbol{x}(z) \stackrel{\text{def}}{=} [X(z)\ X(-z)]^\top, \boldsymbol{q}(z) \stackrel{\text{def}}{=} [Q(z)\ Q(-z)]^\top, \boldsymbol{g}(z) \stackrel{\text{def}}{=} 2[H_0^p(z)\ -H_1^p(z)]^\top$ and the diagonal matrices

$$\boldsymbol{S}(z) \stackrel{\text{def}}{=} \text{diag}\{S(z), S(-z)\},$$
$$\boldsymbol{C}(z) \stackrel{\text{def}}{=} \text{diag}\{C_{1,1}(z), C_{2,2}(z)\}, \quad \text{and}$$
$$\boldsymbol{H}(z) \stackrel{\text{def}}{=} \begin{bmatrix} H_0^p(z) & H_1^p(z) \\ H_1^p(z) & H_0^p(z)\end{bmatrix}.$$

We then have [4] $E(z) = \frac{1}{2}\,\boldsymbol{g}^T(z)([\boldsymbol{H}(z)\boldsymbol{S}(z) - \boldsymbol{C}(z^2)\boldsymbol{H}(z)]\boldsymbol{x}(z) + \boldsymbol{H}(z)\boldsymbol{q}(z))$, which on the unit circle yields

$$\begin{aligned} E(\theta) = {} & ([H_0^{2p}(\theta) - H_1^{2p}(\theta)]S(\theta) \\ & - [H_0^{2p}(\theta)C_{1,1}(2\theta) - H_1^{2p}(\theta)C_{2,2}(2\theta)])X(\theta) \\ & - H_0^{2p}(\theta)H_1^{2p}(\theta)[C_{1,1}(2\theta) - C_{2,2}(2\theta)]X(\theta-\pi) \\ & + [H_0^{2p}(\theta) - H_1^{2p}(\theta)]Q(\theta). \end{aligned} \tag{9}$$

From Theorem 1, the last term in (9) is the near-end signal reconstructed with a notch at $\theta = (\pi/2)$. Note that the near-end signal is reconstructed without aliasing. The second term is due to the aliasing of the loudspeaker signal. Let us evaluate (9) at $\theta = (\pi/2)$ and use Theorem 1. We have

$$\begin{aligned} E\left(\frac{\pi}{2}\right) = -\Big[& H_0^{2p}\left(\frac{\pi}{2}\right)C_{1,1}(\pi) \\ & - H_1^{2p}\left(\frac{\pi}{2}\right)C_{2,2}(\pi)\Big]X\left(\frac{\pi}{2}\right) \\ & - H_0^{2p}\left(\frac{\pi}{2}\right)H_1^{2p}\left(\frac{\pi}{2}\right)[C_{1,1}(\pi) \\ & - C_{2,2}(\pi)]X\left(-\frac{\pi}{2}\right). \end{aligned} \tag{10}$$

Clearly, if

$$\boxed{C_{1,1}(\pi) = C_{2,2}(\pi)} \tag{11}$$

all terms in (10) vanish, and we have $E((\pi/2)) = 0$. Therefore, if the *continuity constraint* in (11) is satisfied, then the residual echo signal at $\theta = (\pi/2)$ is identically zero. Furthermore, since the notch due to the CPS-IIR filter bank has a nonzero transition band, the spectral components around $\theta = (\pi/2)$ will also be attenuated.

V. Continuity Constrained NLMS (CC-NLMS) Algorithm

In the four-band binary-tree decomposition in Fig. 3, the continuity constraints across the subband edges are $a = \tilde{a}, b = \tilde{b}$, and $c = \tilde{c}$. At the reduced rate, these are constraints are at $\theta = 0$ and $\theta = \pi$, and in terms of the adaptive filters $W_i, i = 1, 2, 3, 4$, they are given by

$$\begin{aligned} & \mathcal{Z}_1^\top W_1(k) = \mathcal{Z}_2^\top W_2(k), \mathcal{K}_2^\top W_2(k) = \mathcal{K}_4^\top W_4(k) \\ & \mathcal{Z}_3^\top W_3(k) = \mathcal{Z}_4^\top W_4(k) \end{aligned} \tag{12}$$

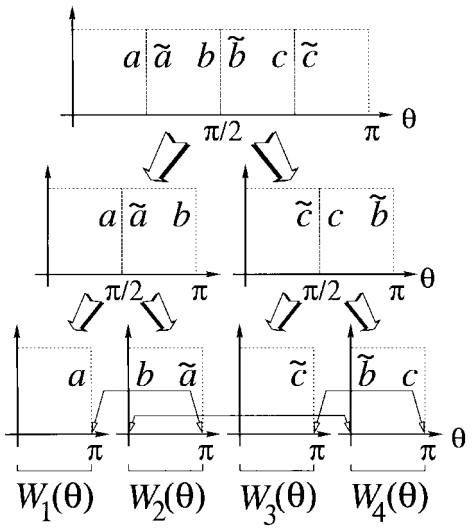

Fig. 3. Four-band binary-tree subband decomposition and the continuity constraints.

where $\mathcal{Z}_i^\top \stackrel{\text{def}}{=} [1\ -1\ 1\ -1\ \cdots]_{1\times L_i}, \mathcal{K}_i^\top \stackrel{\text{def}}{=} [1\ 1\ 1\ 1\ \cdots]_{1\times L_i}$ and $L_i, i = 1, 2, 3, 4$ are the number of adaptive coefficients in each subband. Note that the continuity constraints are mild in the sense that the adaptive coefficients are only forced to be spectrally continuous across the subbands.

Consider the overall cost function

$$\begin{aligned}\hat{\Sigma}_J = \frac{1}{2}\sum_{i=1}^{4}\Bigg(&\|W_i(k)-W_i(k-1)\|_2^2 \\ &-\frac{1}{\|X_i(k)\|_2^2}\left[X_i^\top(k)W_i(k)-y_i(k)\right]^2\Bigg) \\ &+\lambda_1[\mathcal{Z}_1^\top W_1(k)-\mathcal{Z}_2^\top W_2(k)]+\lambda_2[\mathcal{K}_2^\top W_2(k) \\ &-\mathcal{K}_4^\top W_4(k)]+\lambda_3[\mathcal{Z}_3^\top W_3(k)-\mathcal{Z}_4^\top W_4(k)] \end{aligned} \tag{13}$$

where $\lambda_1, \lambda_2,$ and λ_3 are the Lagrange multipliers, $y_i(k) = X_i^\top(k)W_i(k-1)$ are the adaptive filter output, and $\|X_i(k)\|_2^2 \stackrel{\text{def}}{=} X_i^\top(k)X_i(k)$. Let us also define $e_i(k) \stackrel{\text{def}}{=} d_i(k) - y_i(k) = (1/\mu_i)\ [X_i^\top(k)W_i(k) - y_i(k)]$. If we omit the constraints, the minimization of (13) will lead to NLMS algorithms running independently in each subband. After taking the derivatives of $\hat{\Sigma}_J$ with respect to $W_i(k)$ and equating to zero, we obtain the update equations

$$W_1(k) = W_1(k-1) + \frac{\mu_1 e_1(k)}{\|X_1(k)\|_2^2}\ X_1(k) - \lambda_1^*\mathcal{Z}_1 \tag{14}$$

$$\begin{aligned}W_2(k) = W_2(k-1) &+ \frac{\mu_2 e_2(k)}{\|X_2(k)\|_2^2}\ X_2(k) \\ &+ \lambda_1^*\mathcal{Z}_2 - \lambda_2^*\mathcal{K}_2\end{aligned} \tag{15}$$

$$W_3(k) = W_3(k-1) + \frac{\mu_3 e_3(k)}{\|X_3(k)\|_2^2}\ X_3(k) - \lambda_3^*\mathcal{Z}_3 \tag{16}$$

$$\begin{aligned}W_4(k) = W_4(k-1) &+ \frac{\mu_4 e_4(k)}{\|X_4(k)\|_2^2}\ X_4(k) \\ &+ \lambda_2^*\mathcal{K}_4 + \lambda_3^*\mathcal{Z}_4\end{aligned} \tag{17}$$

where $\lambda_1^*, \lambda_2^*, \lambda_3^*$ are the optimal Lagrange multipliers.

We now make use of the continuity constraints in (12) by calculating $\mathcal{Z}_1^\top(14) - \mathcal{Z}_2^\top(15), \mathcal{K}_2^\top(15) - \mathcal{K}_4^\top(17)$, and $\mathcal{Z}_3^\top(16) - \mathcal{Z}_4^\top(17)$. Note that we also use $\mathcal{Z}_1^\top W_1(k-1) = \mathcal{Z}_2^\top W_2(k-1), \mathcal{K}_2^\top W_2(k-1) = \mathcal{K}_4^\top W_4(k-1)$, and $\mathcal{Z}_3^\top W_3(k-1) = \mathcal{Z}_4^\top W_4(k-1)$ as the continuity constraints at the previous instant. Therefore, it is required that the adaptive coefficients are initialized such that these constraints are satisfied. This can be achieved simply by initializing all coefficients to zero. These manipulations lead to

$$\begin{aligned}&\begin{bmatrix} L_1+L_4 & -\mathcal{Z}_2^\top\mathcal{K}_2 & 0 \\ -\mathcal{K}_2^\top\mathcal{Z}_2 & L_2+L_4 & \mathcal{K}_4^\top\mathcal{Z}_4 \\ 0 & \mathcal{Z}_4^\top\mathcal{K}_4 & L_3+L_4 \end{bmatrix}\begin{bmatrix}\lambda_1^* \\ \lambda_2^* \\ \lambda_3^*\end{bmatrix} \\ &\quad= \begin{bmatrix} \dfrac{\mu_1 e_1(k)}{\|X_1(k)\|_2^2}\ \mathcal{Z}_1^\top X_1(k) - \dfrac{\mu_2 e_2(k)}{\|X_2(k)\|_2^2}\ \mathcal{Z}_2^\top X_2(k) \\ \dfrac{\mu_2 e_2(k)}{\|X_2(k)\|_2^2}\ \mathcal{K}_2^\top X_2(k) - \dfrac{\mu_4 e_4(k)}{\|X_4(k)\|_2^2}\ \mathcal{K}_4^\top X_4(k) \\ \dfrac{\mu_3 e_3(k)}{\|X_3(k)\|_2^2}\ \mathcal{Z}_3^\top X_3(k) - \dfrac{\mu_4 e_4(k)}{\|X_4(k)\|_2^2}\ \mathcal{Z}_4^\top X_4(k)\end{bmatrix}.\end{aligned} \tag{18}$$

If L_2 and L_4 are chosen as even numbers, then $\mathcal{Z}_2^\top\mathcal{K}_2 = 0$, and $\mathcal{Z}_4^\top\mathcal{K}_4 = 0$. Since the matrix on the left-hand side of (18) becomes diagonal, λ_i^* can be solved in a straightforward manner. Note that a safety constant $\nu_i > 0$ can be added to each normalization factor $\|X_i(k)\|_2^2$, and this does not violate the continuity constraints. The CC-NLMS adaptive algorithm for eight subbands is tabulated in Table II.

The terms $(\mu_i e_i(k)/\|X_i(k)\|_2^2)X_i(k)$ are already computed in (14)–(17). Therefore, no multiplication operations are required in order to compute λ_i^*. However, further addition/subtraction operations are necessary. Compared with NLMS algorithms running independently in four subbands, the increase in the number of real addition/subtraction operations is given by $\frac{1}{4}\ (9 + 2\ \Sigma_{i=1}^4\ L_i)$ at the full rate.

VI. Simulations

Experiments are conducted where the level of echo cancellation is measured by using the segmental echo return loss enhancement: S-ERLE(i) $\stackrel{\text{def}}{=} 10\log_{10}\ ((\Sigma_{k=(i-1)S}^{iS-1}\ d^2(k)/\Sigma_{k=(i-1)S}^{iS-1}\ e^2(k))), i = 1, \cdots,$ where

- S window size;
- $d(k)$ microphone signal;
- $e(k)$ corresponding fullband residual echo signal.

The maximum and the mean values of S-ERLE(i) are computed over i. The time of initial convergence (TIC) is also measured as the time elapses until S-ERLE(i) = 10 dB. Four techniques are used for echo cancellation. First, the PR-FIR filter in Fig. 1 and the NLMS algorithm are used. Second, subband decomposition is performed by PS-IIR filter banks. Third, the previous technique is used with the DNF's [4] whose parameters are given in Section V. Finally, the proposed CPS-IIR filter banks are used with the CC-NLMS algorithm presented in Section V.

Experiment 1: The loudspeaker signal is chosen as zero-mean and white with unity variance. A 256-tap car cockpit echo path impulse response is used [4]. The number of subbands is 4, and the step sizes in each subband are chosen as 0.5. Each subband adaptive filter has 64 coefficients.

The amplitude spectra of the residual echo signals after convergence are illustrated in Fig. 4. In Fig. 4(a), for a PR-FIR + NLMS technique, the residual echo signal has high-energy components at the subband edges. In Fig. 4(b), with PS-IIR filters, these components have narrower bandwidth but similar peak values. DNF's inserted, as described in [4], lead to the improved state in Fig. 4(c), where the notches are clearly visible. Finally, for the proposed CPS-IIR + CC-NLMS technique in Fig. 4(d), the notches at the subband edges are again clearly visible. The notches in Fig. 4(d) are less pronounced than the notches in Fig. 4(c). This can be expected since in the former case, the DNF's remove energy from the loudspeaker and microphone signals as a preprocessing operation [4]. In the proposed CPS-IIR + CC-NLMS technique, however, the notches are only formed after

TABLE II
EIGHT-BAND CC-NLMS ALGORITHM

Initialisation:	$W_i(0) = \mathbf{0}_{L_i},\ i = 1, \ldots, 8,\ L_i$: even
Constraints:	$\mathcal{Z}_1^\top W_1(k) = \mathcal{Z}_2^\top W_2(k),\ \mathcal{K}_2^\top W_2(k) = \mathcal{K}_4^\top W_4(k)$ $\mathcal{K}_3^\top W_3(k) = \mathcal{K}_7^\top W_7(k),\ \mathcal{Z}_3^\top W_3(k) = \mathcal{Z}_4^\top W_4(k)$ $\mathcal{Z}_5^\top W_5(k) = \mathcal{Z}_6^\top W_6(k),\ \mathcal{K}_6^\top W_6(k) = \mathcal{K}_8^\top W_8(k)$ $\mathcal{Z}_7^\top W_7(k) = \mathcal{Z}_8^\top W_8(k)$
Update equations:	$e_i(k) = d_i(k) - X_i^\top(k) W_i(k-1),\ i = 1, \ldots, 8$

$$\lambda_1^* = \frac{1}{L_1+L_2}\left(\frac{\mu_1 e_1(k)}{\nu_1+\|X_1(k)\|_2^2}\mathcal{Z}_1^\top X_1(k) - \frac{\mu_2 e_2(k)}{\nu_2+\|X_2(k)\|_2^2}\mathcal{Z}_2^\top X_2(k)\right)$$
$$\lambda_2^* = \frac{1}{L_2+L_4}\left(\frac{\mu_2 e_2(k)}{\nu_2+\|X_2(k)\|_2^2}\mathcal{K}_2^\top X_2(k) - \frac{\mu_4 e_4(k)}{\nu_4+\|X_4(k)\|_2^2}\mathcal{K}_4^\top X_4(k)\right)$$
$$\lambda_3^* = \frac{1}{L_3+L_7}\left(\frac{\mu_3 e_3(k)}{\nu_3+\|X_3(k)\|_2^2}\mathcal{K}_3^\top X_3(k) - \frac{\mu_7 e_7(k)}{\nu_7+\|X_7(k)\|_2^2}\mathcal{K}_7^\top X_7(k)\right)$$
$$\lambda_4^* = \frac{1}{L_3+L_4}\left(\frac{\mu_3 e_3(k)}{\nu_3+\|X_3(k)\|_2^2}\mathcal{Z}_3^\top X_3(k) - \frac{\mu_4 e_4(k)}{\nu_4+\|X_4(k)\|_2^2}\mathcal{Z}_4^\top X_4(k)\right)$$
$$\lambda_5^* = \frac{1}{L_5+L_6}\left(\frac{\mu_5 e_5(k)}{\nu_5+\|X_5(k)\|_2^2}\mathcal{Z}_5^\top X_5(k) - \frac{\mu_6 e_6(k)}{\nu_6+\|X_6(k)\|_2^2}\mathcal{Z}_6^\top X_6(k)\right)$$
$$\lambda_6^* = \frac{1}{L_6+L_8}\left(\frac{\mu_6 e_6(k)}{\nu_6+\|X_6(k)\|_2^2}\mathcal{K}_6^\top X_6(k) - \frac{\mu_8 e_8(k)}{\nu_8+\|X_8(k)\|_2^2}\mathcal{K}_8^\top X_8(k)\right)$$
$$\lambda_7^* = \frac{1}{L_7+L_8}\left(\frac{\mu_7 e_7(k)}{\nu_7+\|X_7(k)\|_2^2}\mathcal{Z}_7^\top X_7(k) - \frac{\mu_8 e_8(k)}{\nu_8+\|X_8(k)\|_2^2}\mathcal{Z}_8^\top X_8(k)\right)$$

$$W_1(k) = W_1(k-1) + \frac{\mu_1 e_1(k)}{\nu_1+\|X_1(k)\|_2^2}X_1(k) - \lambda_1^*\mathcal{Z}_1$$
$$W_2(k) = W_2(k-1) + \frac{\mu_2 e_2(k)}{\nu_2+\|X_2(k)\|_2^2}X_2(k) + \lambda_1^*\mathcal{Z}_2 - \lambda_2^*\mathcal{K}_2$$
$$W_3(k) = W_3(k-1) + \frac{\mu_3 e_3(k)}{\nu_3+\|X_3(k)\|_2^2}X_3(k) - \lambda_3^*\mathcal{K}_3 - \lambda_4^*\mathcal{Z}_3$$
$$W_4(k) = W_4(k-1) + \frac{\mu_4 e_4(k)}{\nu_4+\|X_4(k)\|_2^2}X_4(k) + \lambda_2^*\mathcal{K}_4 + \lambda_4^*\mathcal{Z}_4$$
$$W_5(k) = W_5(k-1) + \frac{\mu_5 e_5(k)}{\nu_5+\|X_5(k)\|_2^2}X_5(k) - \lambda_5^*\mathcal{Z}_5$$
$$W_6(k) = W_6(k-1) + \frac{\mu_6 e_6(k)}{\nu_6+\|X_6(k)\|_2^2}X_6(k) + \lambda_5^*\mathcal{Z}_6 - \lambda_6^*\mathcal{K}_6$$
$$W_7(k) = W_7(k-1) + \frac{\mu_7 e_7(k)}{\nu_7+\|X_7(k)\|_2^2}X_7(k) + \lambda_3^*\mathcal{K}_7 - \lambda_7^*\mathcal{Z}_7$$
$$W_8(k) = W_8(k-1) + \frac{\mu_8 e_8(k)}{\nu_8+\|X_8(k)\|_2^2}X_8(k) + \lambda_6^*\mathcal{K}_8 + \lambda_7^*\mathcal{Z}_8$$

TABLE III
EXPERIMENTAL RESULTS WITH WHITE INPUT SIGNAL. THE NUMBER OF SUBBANDS IS 4

Technique	Max(S-ERLE) (dB)	Mean(S-ERLE) (dB) at the steady-state
PR-FIR + NLMS	10.57	9.81
PS-IIR + NLMS	15.29	14.01
PS-IIR + DNF + NLMS [4]	26.38	25.84
CPS-IIR + CC-NLMS	23.01	22.05

TABLE IV
EXPERIMENTAL RESULTS WITH REAL SPEECH RECORDINGS. THE NUMBER OF SUBBANDS IS 4

Technique	Max(S-ERLE) (dB)	Mean(S-ERLE)	TIC-10dB (msec.)
PR-FIR + NLMS	20.53	11.27	112.0
PS-IIR + NLMS	21.14	11.88	80.0
PS-IIR + DNF + NLMS [4]	22.34	13.48	80.0
CPS-IIR + CC-NLMS	22.12	13.02	80.0

adaptive filtering at the output of the synthesis bank. The results are summarized in Table III.

Experiment 2: Experiments are conducted with female and male speech signals recorded in a car at 8-KHz sampling frequency under the single-talk condition. The step sizes and the lengths of the adaptive filters are the same as in the previous experiment. The results are presented in Table IV, where Max(S-ERLE), Mean(S-ERLE), and TIC-10dB are provided, with $S = 250$ corresponding to 32-ms windows. The results indicate that the performance of the proposed CPS-IIR + CC-NLMS technique is close to the performance of the PS-IIR + DNF + NLMS technique. The PR-FIR + NLMS technique yields the lowest ERLE performance and the slowest convergence behavior.

VII. CONCLUSIONS

Power symmetric IIR filters are used in cascade form, and new analysis and synthesis banks are proposed that can be implemented in polyphase form. It is shown that when the number of cascades is even, there is a notch at the subband division frequency at the output of the analysis bank followed by the synthesis bank. The bandwidth

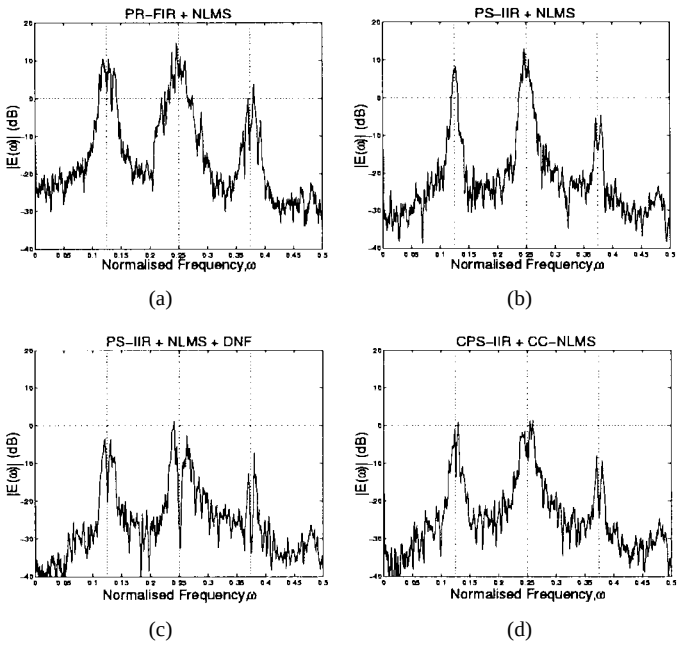

Fig. 4. Amplitude spectrum of the residual echo for (a) PR-FIR + NLMS. (b) PS-IIR + NLMS. (c) PS-IIR + DNF + NLMS. (d) CPS-IIR + CC-NLMS technique $\omega = (\theta/2\pi)$.

of the notch is estimated in terms of the allpass parameters of the prototype PS-IIR filter. By investigating the generic two-band AEC, it is shown that the adaptive filters in the neighboring subbands must be coupled via continuity constraints. The NLMS algorithm is modified, and the CC-NLMS algorithm is proposed. The experimental results validate the anticipated attenuation of the aliased spectrum around the subband division frequencies.

The continuity constraints in the proposed technique are *pointwise* constraints that are enforced only at the subband edges. More well-defined notches can be obtained, i) by further imposing the continuity of the derivatives of the spectrum at the subband edges and ii) by forcing a higher number of continuity constraints in a narrowband around each subband division frequency. Both alternatives can be considered within the same Lagrange optimization framework. Various implementations of least-squares adaptive algorithms can be modified with continuity constraints for faster convergence and a higher level of echo cancellation.

ACKNOWLEDGMENT

The authors thank the coordinating editor and the reviewers for their comments.

REFERENCES

[1] E. Hansler, "The hands-free telephone problem: A second annotated bibliography update," in *Int. Workshop Acoust. Echo Noise Contr.*, Roros, Norway, June 1995, pp. 107–114.

[2] W. Kellermann, "Analysis and design of multirate systems for cancellation of acoustical echoes," in *ICASSP*, New York, Apr. 1988, pp. 2570–2573.

[3] A. Gilloire and M. Vetterli, "Adaptive filtering in sub-bands with critical sampling: Analysis, experiments and application to acoustic echo cancellation," *IEEE Trans. Signal Processing*, vol. 40, pp. 1862–1875, Aug. 1992.

[4] O. Tanrikulu, B. Baykal, A. G. Constantinides, and J. A. Chambers, "Residual signal in critically sampled subband acoustic echo cancellers based on IIR and FIR filter banks," *IEEE Trans. Signal Processing*, vol. 45, pp. 901–912, Apr. 1997.

[5] P. P. Vaidyanathan, *Multi-rate Systems and Filter Banks*. Englewood Cliffs, NJ: Prentice-Hall, 1993.

[6] T. Q. Nguyen, T. L. Laakso, and D. Koilpillai, "Eigenfilter approach for the design of allpass filters approximating a given phase response," *IEEE Trans. Signal Processing*, vol. 42, pp. 2257–2263, Sept. 1994.

[7] P. P. Vaidyanathan, S. K. Mitra, and Y. Neuvo, "A new approach to the realization of low-sensitivity IIR digital filters," *IEEE Trans. Acoust., Speech, Signal Processing*, vol. ASSP-34, pp. 350–361, Apr. 1986.

[8] P. A. Regalia, S. K. Mitra, and P. P. Vaidyanathan, "The digital all-pass filter: A versatile signal processing building block," *Proc. IEEE*, vol. 76, pp. 19–37, Jan. 1988.

Fast Ambiguity Processing in SOFAR Propagation Involving Periodic Signals and M Sequences

Didier Mauuary, Genevive Jourdain, and T. Terre

***Abstract*—Fast ambiguity processing can be used in active time delay and Doppler identification in the sound fixing and ranging (SOFAR) propagation context. They need periodic signals generated from pseudo-random M sequences. In the particular case of the SOFAR, the range of the observed Doppler effect enables use of the fastest version, provided that the periodicity of the signal is correctly adjusted.**

***Index Terms*—Computational complexity, delay-Doppler ambiguity, M sequences, periodic signals, SOFAR propagation.**

I. INTRODUCTION

A high delay-Doppler resolution signal having good propagating properties in the sound fixing and ranging (SOFAR) channel is generally a wideband signal modulated around a carrier frequency f_0. Its complex analytic form is

$$s(t) = \overline{s}(t)\ \exp(j2\pi f_0 t), \qquad 0 < t < \mathcal{T}. \tag{1}$$

$\overline{s}(t)$ stands for the complex envelope of the signal of duration $\mathcal{T}$. The received analytic signal $r(t)$ is of the form $s(t-\tau)$, where τ is the propagation delay. In this correspondence, first-order Doppler effect, i.e., a linear variation of delay $\tau(t)$, is considered:

$$r(t) = s(t-\tau(t)) = \overline{s}(\xi t - \tau_0)\ \exp(j2\pi f_0 \xi t) \tag{2}$$

where $\xi = 1-\mu$ stands for the Doppler stretch factor and τ_0 for the delay at $t = 0$. Complex attenuation, as well as multipath effect, is not explicitly written. Therefore, the baseband (i.e., f_0-demodulated) signal $\overline{r}(t)$ has a residual frequency shift equal to $-f_0\mu$. μ is the normalized Doppler.

The main characteristic of the acoustic waves in the SOFAR channel is that they are axial waves: The elevation angles of the eigenrays, connecting a source to a receiver, are limited in magnitude.

Manuscript received November 2, 1996; revised January 12, 1998. The associate editor coordinating the review of this paper and approving it for publication was Prof. Hagit Messer-Yaron.

D. Mauuary and G. Jourdain are with CEPHAG (URA CNRS 346), Saint Martin d'Hères, France (e-mail: Didier.Mauuary@lis.inpg.fr).

T. Terre is with IFREMER (LPO), Plouzané, France.

Publisher Item Identifier S 1053-587X(98)05233-7.